ACS APPLIED MATERIALS & INTERFACES

Letter

www.acsami.org

# Dye-Sensitization-Induced Visible-Light Reduction of Graphene Oxide for the Enhanced $TiO_2$ Photocatalytic Performance

Ping Wang,[†] Jin Wang,[†] Tingsen Ming,[†] Xuefei Wang,[†] Huogen Yu,*[,†] Jiaguo Yu,[‡] Yonggang Wang,[§] and Ming Lei*[,§]

[†]Department of Chemistry, School of Science, and [‡]State Key Laboratory of Advanced Technology for Materials Synthesis and Processing, Wuhan University of Technology, Wuhan 430070, People's Republic of China

[§]School of Science, Beijing University of Posts and Telecommunications, Beijing 100876, People's Republic of China

Supporting Information

**ABSTRACT:** The reduction of graphene oxide (GO) with a large-scale production has been demonstrated to be one of the key steps for the preparation of graphene-based composite materials with various potential applications. Therefore, it is highly required to develop a facile, green, and environmentally friendly route for the effective reduction of GO. In this study, a new and effective reduced method of GO nanosheets, based on the dye-sensitization-induced visible-light reduction mechanism, was developed to prepare reduced GO (rGO) and graphene-based $TiO_2$ composite in the absence of any additional reducing agents. It was found that the dye-sensitization-induced reduction process of GO was accompanied with the formation of $TiO_2$-rGO composite nanostructure. The photocatalytic experimental results indicated that the resultant $TiO_2$-rGO nanocomposites exhibited significantly higher photocatalytic performance than pure $TiO_2$ because of a rapid separation of photogenerated electrons and holes by the rGO cocatalyst.

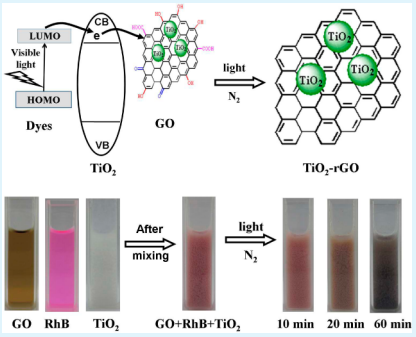


**KEYWORDS:** *graphene, $TiO_2$-rGO, photocatalysis, dye-sensitization-induced, interface*

## 1. INTRODUCTION

Graphene, an atomic sheet of $sp^2$-bonded carbon atoms, is a promising material for various applications because of its unique structure and property such as high electron mobility (250,000 $cm^2\ V^{-1}\ s^{-1}$) and high surface area (2630 $m^2/g$).[1−3] However, the high-quality graphene obtained from the manual mechanical cleavage of graphite is not suitable for large-scale applications because of its low synthetic efficiency.[4] Recently, it was demonstrated that the reduction of graphene oxide (GO) nanosheets was an effective route to produce high-quality and large-scale graphene.[5,6] However, preparing from graphite via strong oxidation process by strong oxidants, the resultant GO nanosheets usually contain various oxygen-containing functional groups and defects, resulting in a low electron transport property.[5,6] Therefore, it is necessary and important to develop various strategies to reduce chemically converted GO to recover its high electron mobility. Various reducing methods such as chemical reduction by using reductants ($N_2H_4$,[7] $NaBH_4$[8] and alcohols[9]), hydrothermal,[10−13] solvothermal,[14,15] microwave-assisted reduction,[16] and supercritical fluid method[17] have been widely used to prepare reduced GO (rGO) to restore the $sp^2$-hybridized network and increase the electronic conductivity. However, these methods have intrinsic shortcomings, such as the involvement of toxic chemical agents, requiring high temperature, and the additives of acid or alkali. It is highly required to develop new and environmental-friendly methods for the reduction of GO nanosheets. Recently, photocatalytic-induced reduction mechanism has been demonstrated to be one of the new, green and effective methods for the reduction of GO. Williams et al. demonstrated the effective reduction of GO by UV-assisted photocatalytic reduction mechanism of $TiO_2$ photocatalyst.[18] In their study, the photogenerated electrons were first produced on the conduction of $TiO_2$ under UV-light irradiation and subsequently transferred to the GO nanosheets, resulting in the formation of rGO. Sun et al. also reported the surface plasmon resonance-induced visible-light photocatalytic reduction of GO by using Ag nanoparticles as a plasmonic photocatalyst.[19] In their study, after absorbing visible light by Ag nanoparticles via surface plasmon resonance, the photogenerated electrons could be injected into the surface of GO nanosheets, leading to the effective reduction of GO. On the other hand, the dye-sensitization-induced electron transfer mechanism has been well recognized and widely used to improve the photon-to-electron conversion efficiency of solar cell.[20] Under visible-light irradiation, the photo-induced electrons on the excited dye can be injected into the anode via semiconductor photocatalysts to produce current. Considering a similar electron transfer mechanism of photocatalytic-induced reduction of GO and dye-sensitized solar cell,[21−23] it is expected that the dye-

Received: March 7, 2013
Accepted: March 27, 2013

 © XXXX American Chemical Society  dx.doi.org/10.1021/am4008566 | ACS Appl. Mater. Interfaces XXXX, XXX, XXX−XXX

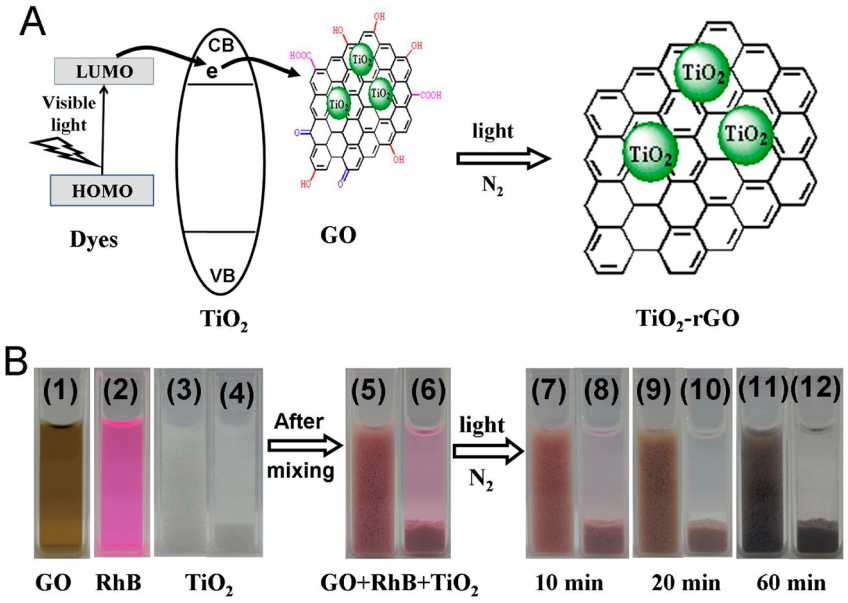


**Figure 1.** (A) Graphical illustration of the dye-sensitization-induced visible-light reduction of GO nanosheets and the following formation of $TiO_2$-rGO composite; (B) photographs of the (1) GO solution, (2) RhB solution, (3, 4) $TiO_2$ suspension (3) before and (4) after aging for 5 min, (5, 6) the mixing solution (5) before and (6) after aging for 5 min, (7, 8) 10-min irradiated mixing solution (7) before and (8) after aging for 5 min, (9, 10) 20-min irradiated mixing solution (9) before and (10) after aging for 5 min, and (11, 12) 60-min irradiated mixing solution (11) before and (12) after aging for 5 min.

sensitization-induced electron transfer mechanism can provide a facile and effective method for the reduction of GO to prepare high-quality graphene-based composite materials.

In this study, we demonstrated a facile and new reduction route of GO nanosheets via dye-sensitization-induced visible-light reduction mechanism. The photocatalytic experimental results show that the resultant rGO can be used as an effective cocatalyst to improve the photocatalytic performance of $TiO_2$ photocatalysts via a rapid separation of photogenerated electrons and holes. To the best of our knowledge, this is the first report about dye-sensitization-induced visible-light reduction of GO without using any reducing agents. This work may provide a facile, promising, and environmentally friendly strategy for the reduction of GO and the preparation of graphene-based composite materials.

## 2. EXPERIMENTAL SECTION

**Materials.** Graphite was provided from Nanjing XFNANO Materials Tech Co Ltd and all the other reagents (analytical grade) were supplied by Shanghai Chemical Reagent Ltd. (P.R. China) and used as received without further purification.

**Preparation of GO.** The graphene oxide was synthesized from natural graphite powder (99.95%).[24] Briefly, 3 g of graphite, 2.5 g of $K_2S_2O_8$ and 2.5 g of $P_2O_5$ were added into 12 mL of concentrated $H_2SO_4$ under strong stirring at 80 °C for 4.5 h. After the solution was cooled down to room temperature naturally, 0.5 L of deionized (DI) water was added into the above solution and aged for 12 h. The suspension was filtered, washed and dried to obtain the black solid. The black solid was mixed with 120 ml of concentrated $H_2SO_4$ and 15 g of $KMnO_4$ in an ice bath below 20 °C, and then was transferred to a water bath and magnetically stirred at 35 °C for 2 h. The resulting dark-brown paste was diluted with the slow addition of 250 ml of DI water and then stirred for another 2 h. A 20 mL (30 wt %) of $H_2O_2$ was slowly added to quench the solution to produce a golden-brown solution. After the resultant product was centrifuged, the sample was washed with HCl (1:10) and DI water, respectively, until the pH of the washed solution was ca. 6. Finally, the product was dried at 40 °C in vacuum to obtain the GO sample. The GO solution was obtained by ultrasonic dispersion of GO in DI water for 2 h.

**Preparation of $TiO_2$-rGO.** The reduction of GO nanosheets was conducted in a mixing suspension solution of GO, Rhodamine B (RhB) dye and $TiO_2$ nanoparticles. The rhodamine B (RhB), a well-known dye with a strong absorption in the visibe light region, was used as the visible-light sensetive dye. Commercial $TiO_2$ nanoparticles (P25 $TiO_2$, Degussa), a well-known photocatalyst with a good dispersion, was pre-treated at 550 °C for 2 h in order to obtain a clean $TiO_2$ surface after the removal of adsorbed substances.

In a typical synthesis, 1 g of P25 $TiO_2$ powder was added into 10 mL of GO solution under stirring at room temperature. After stirring for 30 min, 5 mL of RhB solution (10 mg $L^{-1}$) was added into the above mixing solution and then stirred for another 30 min to form a homogenerous suspension solution. The resultant suspension solution was then bubbled with nitrogen gas to remove the oxygen in the solution. After bubbling for 30 min, the suspension solution was irradiated under visible-light condition for 60 min. With increasing irradiation time, the color of the suspension changed from pink to black gradually, suggesting the effective reductin of GO to rGO. After the formation of black suspension, the resultant sample was recovered by filtration, rinsed with DI water and then dired at 60 °C to obtain the $TiO_2$-rGO nanocomposites. The weight ratio of rGO to $TiO_2$ can be controlled to be 0, 0.1, 0.5, 1, and 5 wt % by the GO solution with a concentration of 0, 0.01, 0.05, 0.1, and 0.5 wt %, respectively. A 350 W xenon lamp equipped with a UV-cutoff filter (providing visible light with $\lambda \geq 400$ nm) was used as a visible-light source.

**Characterization.** X-ray diffraction (XRD) patterns were obtained on a D/MAX-RBX-ray diffractometer (Rigaku, Japan). X-ray photoelectron spectroscopy (XPS) measurements were done on a KRATOA XSAM800 XPS system with Mg K$\alpha$ source. Morphological analysis was performed with an S-4800 field emission scanning electron microscope (FESEM) (Hitachi, Japan) and JEM-2100F transmission electron microscopy (TEM) (JEOL, Japan). Raman spectra were collected using an INVIA spectrophotometer (Renishaw, UK). Fourier Transform Infrared spectra (FTIR) were acquired using a Nexus FT-IR spectrophotometer (Thermo Nicolet, America). UV-vis absorption spectra were obtained using a UV−visible spectrophotometer (UV-2550, SHI- MADZU, Japan).


dx.doi.org/10.1021/am4008566 | ACS Appl. Mater. Interfaces XXXX, XXX, XXX−XXX

**Photocatalytic activity.** The evaluation of photocatalytic activity of the prepared samples for the photocatalytic decomposition of methyl orange (MO) and dimethyl phthalate (DMP) aqueous solutions was performed at ambient temperature.[25,26] Experimental details were shown as follows: 50 mg of the sample was dispersed into 10 ml of MO solution (20 mg $L^{-1}$) or DMP solution (20 mg/L) in a disk with a diameter of ca. 5 cm. The mixed suspension was placed in dark for 3 h to reach the adsorption-desorption equilibrium between the photocatalyst and MO (or DMP) before irradiation. The integrated UV intensity in the range of 310-400 nm striking the sample, measured with a UV radiometer (Model: UV-A, made in Photoelectric Instrument Factory of Beijing Normal University), was 2.5 mW/$cm^2$ with a peak wavelength of 365 nm. The concentration of MO (or DMP) was determined by an UV−visible spectrophotometer (UV-1240, SHIMADZU, Japan). After light irradiation for some time, the reaction solution was centrifuged to measure the concentration of MO (or DMP). As for the MO (or DMP) aqueous solution with low concentration, its photocatalytic decolorization is a pseudo-first-order reaction and its kinetics may be expressed as $\ln(c/c_0) = -kt$, where $k$ is the apparent rate constant, and $c_0$ and $c$ are the MO (or DMP) concentrations at initial state and after irradiation for $t$ min, respectively.[27,28]

## 3. RESULTS AND DISCUSSION

**Strategy for the Synthesis of $TiO_2$-rGO.** Figure 1A displays the graphical illustration of the dye-sensitization-induced visible-light reduction of the GO nanosheets for the preparation of $TiO_2$-rGO composite. Based on the dye-sensitization mechanism, the photogenerated electrons are first produced on the excited dye molecule under visible light illumination and then transferred to the GO via the conduction band of $TiO_2$, leading to the effective reduction of GO to rGO. Considering the electron transfer route from excited dye to GO nanosheets via $TiO_2$ nanoparticles, it is clear that the well coupled interface between the $TiO_2$ and GO nanosheets is significantly critical for the effective reduction of GO nanosheets.

Figure 1B shows the photographs of the GO reduction and the formation process of $TiO_2$-rGO composite materials. The GO can be well dispersed into water to form a homogeneous and stable brown solution owing to the existing of a lot of oxygenous groups such as −OH, C═O, C−O−C, and −COOH (Figure 1B-(1)),[29] whereas a $TiO_2$ colloid suspension is usually obtained because of its small nanoparticles and good dispersion (Figure 1B-(3)). When the P25 $TiO_2$ powder is dispersed into the mixing solution of RhB and GO, a homogeneous $TiO_2$-GO suspension with a cottonlike structure can be observed (Figure 1B-(5)). After aging for 5 min without stirring, it is interesting to find that the resultant cotton-like suspension can precipitate completely on the bottom of bottle and the residual solution is very clear (Figure 1B-(6)). This phenomenon is completely different from the single-component $TiO_2$ suspension with a milk-like colloid solution after aging for 5 min (Figure 1B-(4)), suggesting that the GO nanosheets can be completely coupled on the surface of $TiO_2$ nanoparticles to form a $TiO_2$-GO composite, resulting in their simultaneous precipitation. The formation of well coupled interface possibly can be ascribed to the fact that the interaction between $TiO_2$ nanoparticles and GO nanosheets is much higher than that of $TiO_2$ nanoparticles (or GO nanosheets) with $H_2O$ molecules owing to their excellent hydrophilicity. In addition, the high adsorption ability of $TiO_2$ nanoparticles with a clean surface after high-temperature calcination also contributes their enhanced interaction with the GO nanosheets. Additional experiments suggested that the GO nanosheets could not be detached from the $TiO_2$ nanoparticles by strong stirring or ultrasonic dispersion of the $TiO_2$-GO precipitate, further suggesting a strong interaction between the GO nanosheets and the $TiO_2$ nanoparticles. Further observation about the mixing solution after aging for 5 min (Figure 1B-(6)) indicates that the color of the residual solution clearly turns into a lighter pink color compared with the RhB precursor solution (Figure 1B-(2)), revealing that most of the RhB dyes are adsorbed on the surface of $TiO_2$-GO composite. The good adsorption of RhB dyes and strongly coupling interaction of $TiO_2$ nanoparticles with the GO nanosheets provide the excellent conditions for the following reduction of GO to rGO via the dye-sensitization-induced visible-light reduction mechanism (Figure 1A).

With increasing visible-light irradiation time, the $TiO_2$-GO composite (Figure 1B-(7,9,11)) gradually changed from light pink to black color due to the in situ reduction of GO on the surface of $TiO_2$ nanoparticles.[30] Simultaneously, the light pink of the residual RhB solution (Figure 1B-(8,10,12)) is decreased and then disappeared completely owing to the photosensitive decomposition of RhB dye. Additional experiment (see Figure S1 in the Supporting Information) suggested that, in the absence of $TiO_2$ particles, the GO nanosheets in the GO-RhB mixing solution cannot be effectively reduced, further demonstrating the dye-sensitization-induced visible-light reduction mechanism via the conduction band of $TiO_2$. In views of the mild reduction conditions in this study, the cotton-like structure and strongly coupled interface of the $TiO_2$-GO composite can be well preserved in the resultant $TiO_2$-rGO composite, which can be well demonstrated by the residual solution with a colorless and clear feature after the pricipation of $TiO_2$-rGO composite (Figure 1B-(12)). In addition, it was also found that after visible-light irradiation the prepared rGO nanosheets could not be detached from the $TiO_2$ nanoparticles by ultrasonic dispersion, furhter indicating the formation of strong coupling interface bewteen the $TiO_2$ nanoparticles and rGO. The cotton-like photocatalyst can be regarded as an ideal and novel photocatalyst with many advantages for the decomposition of organic substances in the aqueous solution such as the good dispersion and easy recovery, while the strongly coupled interface can promote the rapid and effective transfer of photogenerated electrons, resulting in an obviously enhanced photocatalytic performance (see below). As a consequence, the one-step formation process of the $TiO_2$-rGO nanocomposites is based on the initial formation of strong-coupling $TiO_2$-GO nanocomposite and the subsequent in-situ reduction of GO to rGO via dye-sensitization-induced visible-light reduction mechanism, as shown in Figure 1A.

**Morphology and Microstructures of $TiO_2$-rGO.** After visible-light irradiation for 60 min in $N_2$ conditions, the color of $TiO_2$ powder was turned into black owing to the formation of $TiO_2$-rGO nanocomposites. In view of mild experimental conditions, the crystal structure about the $TiO_2$ precursor can be well preserved based on the XRD results (see Figure S2 in the Supporting Information). Images a and b in Figure 2 show the typical SEM and TEM images of the $TiO_2$-rGO composite, respectively. Usually, a crumpled graphene nanostructure is observed owing to its thin and larger sheetlike morphology, whereas the P25 $TiO_2$ is composed of many small nanoparticles with a size of 10−50 nm. As for the $TiO_2$-rGO nanocomposite, the surface of $TiO_2$ nanoparticles is covered by rGO nanosheets, leading to the formation of an interconnected network of $TiO_2$-rGO nanocomposite (Figure 2).


dx.doi.org/10.1021/am4008566 | ACS Appl. Mater. Interfaces XXXX, XXX, XXX−XXX

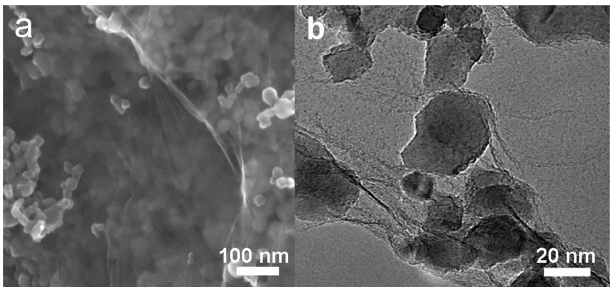


**Figure 2.** (a) FESEM and (b) TEM images of the $TiO_2$-rGO (5 wt %).

The effective reduction of GO to rGO and the successful preparation of the $TiO_2$-rGO composites via the dye-sensitization-induced visible-light reduction mechanism can be further demonstrated by the FTIR, Raman, XPS, and UV-vis spectra technologies. Figure 3a shows the FTIR spectra of GO,

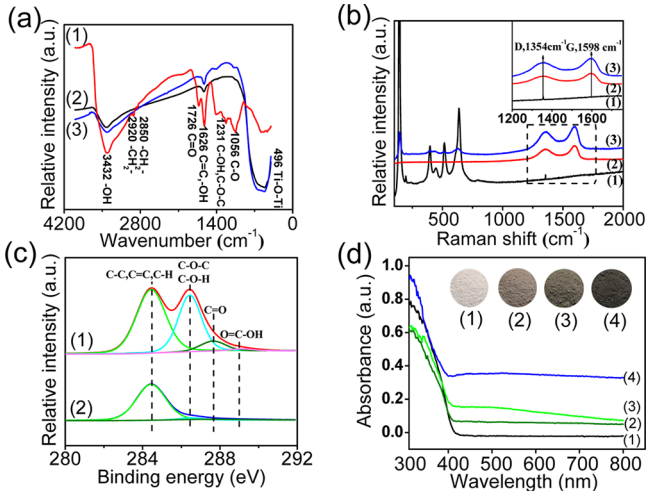


**Figure 3.** (a) FTIR spectra of (1) GO, (2) $TiO_2$, and (3) $TiO_2$-rGO (5 wt %); (b) Raman spectra of (1) $TiO_2$, (2) GO, and (3) $TiO_2$-rGO (5 wt %); (c) XPS spectra of C 1s of (1) GO, and (2) $TiO_2$-rGO (5 wt %); (d) UV-vis diffuse spectra of (1) $TiO_2$, (2) $TiO_2$-rGO (0.1 wt %), (3) $TiO_2$-rGO (0.5 wt %), and (4)$TiO_2$-rGO (5 wt %).

$TiO_2$ and $TiO_2$-rGO samples. It is clear that the GO (Figure 3(a-1)) shows many strong absorption peaks corresponding to various oxygen functional groups, such as water −OH stretching (3410 $cm^{-1}$),[31] carboxylates or ketones C═O stretching (1734 $cm^{-1}$),[32,33] water −OH bending, and C═C stretching (1629 $cm^{-1}$),[34,35] alcoholic C−OH bending (1420 $cm^{-1}$),[34,35] epoxide C−O−C or phenolic C−O−H stretching (1227 $cm^{-1}$), and C−O stretching (1055 $cm^{-1}$).[36,37] For the $TiO_2$ nanoparticles (Figure 3(a-2)), the absorption peaks at 3410 and 1629 $cm^{-1}$ come from the water −OH group, whereas the wide peaks at 400−900 $cm^{-1}$ is attributed to the stretching vibration of Ti−O−Ti bonds in crystalline $TiO_2$.[38] After visible-light irradiation in $N_2$ atmosphere, the intensity of absorption peaks corresponding to oxygen functional groups (C═O peak at 1734 $cm^{-1}$, alcoholic C−OH peak at 1420 $cm^{-1}$, epoxide C−O−C or phenolic C−O−H stretching at 1227 $cm^{-1}$, C−O peak at 1055 $cm^{-1}$) has a significant decrease in the resulting $TiO_2$-rGO (Figure 3(a-3)) compared with the GO (Figure 3(a-1)), suggesting the effective reduction of GO to rGO.

Raman spectroscopy can provide further information about the formation of $TiO_2$-rGO composite, as shown in Figure 3b. It is clear that $TiO_2$ shows strong Raman characteristic peaks at 146 $cm^{-1}$ ($E_{g(1)}$), 397 $cm^{-1}$ ($B_{1g}$), 517 $cm^{-1}$ ($A_{1g}$), and 636 $cm^{-1}$ ($E_{g(2)}$) modes (Figure 3(b-1)).[39] After coupling with rGO (Figure 3(b-3)), the intensity of the four characteristic peaks of $TiO_2$ shows a significant decrease. The possible reasons can be attributed to the fact that the surface of $TiO_2$ is homogeneously wrapped by rGO and there is a strong chemical interaction between $TiO_2$ and rGO sheets. In addition, Raman spectroscopy is also a powerful and widely used method for the characterization of $sp^2$- and $sp^3$-hybridized carbon atoms in graphene to distinguish the order and disorder/defect structures.[34] The Raman spectra of GO and $TiO_2$-rGO show the characteristic D band at 1354 $cm^{-1}$ and G band at 1598 $cm^{-1}$, as shown in the inset of Figure 3b. The G band corresponds to the first-order scattering of the $E_{2g}$ mode observed for $sp^2$ carbon domains, whereas the D band is attributed to a breathing mode of $\kappa$-point phonons of $A_{1g}$ symmetry, which is a common feature of $sp^3$ defects in carbon and usually can be associated with the structural defects, amorphous carbon, or edges that break the symmetry and selection rule.[10] Therefore, the intensity ratio of the D band to the G band is usually a measure of the disorder/defects in graphene, and a smaller intensity ratio of $I_D/I_G$ can be assigned to fewer $sp^3$ defects/disorders and larger average size (or less amount) of the in-plane graphitic crystallite $sp^2$ domains.[34] Compared with the GO (0.807), the calculated $I_D/I_G$ of the $TiO_2$-rGO is 0.840, suggesting the formation of more $sp^3$ defects in the rGO. Considering a deoxygenation/reduction process, it is clear that the defects in the GO nanosheets cannot be well repaired by the dye-sensitization-induced visible-light reduction mechanism. However, compared to the dramatically increased $I_D/I_G$ ratio of the rGO prepared from the hydrazine monohydrate, the increased number of $sp^3$ defects caused by the hydrothermal method is still very limited.[40] In fact, the possible reason for the increased $sp^3$ defects can be attributed to the strong interaction between the interface of $TiO_2$ nanoparticles and rGO nanosheets.

Figure 3(c-1) showed the XPS spectrum of C 1s in the GO and $TiO_2$-rGO. The C 1s peak in the XPS spectrum shows the presence of four types of carbon bonds, that is, the non-oxygenated ring C (284.5 eV, including C−C, C═C, and C−H), the C−O in C−O−C or C−OH groups (286.5 eV), the carbonyl C in C═O (287.8 eV) and the carboxylate carbon in O═C−OH (289.0 eV), suggesting a considerable degree of oxidation for the GO nanosheets.[41] After dye-sensitization-induced visible-light reduction of GO nanosheets, the XPS peak intensity of these carbon−oxygen species in the resulting $TiO_2$-rGO composite (Figure 3(c-2)) shows a dramatic decrease, suggesting the effective deoxygenation of GO nanosheets. To further illustrate the dye-sensitization-induced visible-light reduction degree of the GO nanosheets, the peak area ratios of oxygen-containing bonds to total area are calculated on the basis of XPS results and the corresponding results are shown in Table 1. It is clear that the amount of oxygen-containing groups such as C−O, C═O, and COOH has a significant decrease, which further provides strong evidence for the reduction of GO in $TiO_2$-rGO composites.

Figure 3d shows the UV−vis spectra of the $TiO_2$-rGO composites. Compared with the P25 $TiO_2$ nanoparticles, the absorption edges of the $TiO_2$-rGO composites almost show no change, suggesting that the rGO was mainly grafted on the


dx.doi.org/10.1021/am4008566 | ACS Appl. Mater. Interfaces XXXX, XXX, XXX−XXX

**Table 1. Peak Area ($A$) Ratios Oxygen-Containing Bonds to Total Area (obtained by XPS)**

| sample | $A_{CC}/A$ | $A_{C-O}/A$ | $A_{C=O}/A$ | $A_{O=C-OH}/A$ |
|---|---|---|---|---|
| GO | 0.54 | 0.38 | 0.07 | 0.01 |
| $TiO_2$-rGO (5 wt %) | 0.91 | 0.05 | 0.04 | 0 |

surface of $TiO_2$, which has no effect on the band structure of precursor $TiO_2$ nanoparticles. With increasing amount of the rGO, the $TiO_2$-rGO composites show a continuously enhanced visible-light absorption in the range of 400-800 nm owing to the grafting of rGO, which is in agreement with the color change from white to black, as shown in the inset of Figure 3d.

**Photocatalytic Performance.** The photocatalytic performance of $TiO_2$ and $TiO_2$-rGO composites was first evaluated by photocatalytic decolorization of MO aqueous solution (Figure 4). It is clear that all the $TiO_2$-rGO nanocomposites

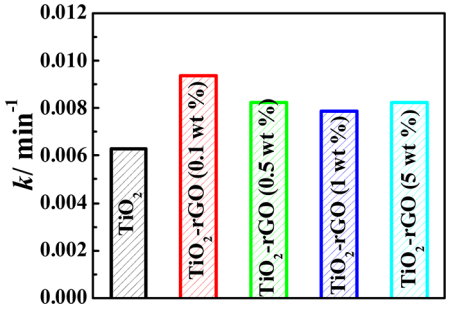


**Figure 4.** Photocatalytic degradation rate constant ($k$) of MO for the $TiO_2$-rGO photocatalysts.

exhibit a higher photocatalytic activity than the pure $TiO_2$ ($k$ = 0.0062 $min^{-1}$). Especially, when the amount of rGO is ca. 0.1 wt %, the resultant $TiO_2$-rGO nanocomposite shows the highest photocatalytic performance with a $k$ value of 0.0095 $min^{-1}$, which is larger than that of pure $TiO_2$ by a factor of 53 %. The enhanced photocatalytic performance of the $TiO_2$-rGO nanocomposites is well-known and can be attributed to the effective transfer and separation of photogenerated electrons by rGO nanosheets.[42−44] Further experimental results suggested that the $TiO_2$-rGO composite photocatalysts also exhibited effective photocatalytic decomposition for colorless dimethyl phthalate solution (see Figure S3 in the Supporting Information), in good agreement with the previous study.[45] Similar to the well-known noble metal-modified semiconductor photocatalysts,[46−48] in this study, the rGO nanosheets work as an effective cocatalyst and functions as an electron sink to accept photogenerated electrons from excited $TiO_2$, resulting in a lower recombination rate and enhanced photocatalytic activity. Further experimental results suggest that when the rGO amount is increased to 10 wt %, the $TiO_2$-rGO nanocomposite shows an obviously decreased photocatalytic activity due to the rapid decrease in irradiation passing through the reaction suspension solution.

## 4. CONCLUSION

In summary, GO could be effectively reduced by a facile and environmentally friendly strategy without using any reducing agents, based on the dye-sensitization-induced reduction mechanism. It was found that the dye-sensitization-induced reduction process of GO was accompanied with the formation of $TiO_2$-rGO composite nanostructure. The photocatalytic experimental results showed that all the $TiO_2$-rGO composites exhibited higher photocatalytic performance than pure $TiO_2$ due to the effective transfer and separation of photogenerated electrons by rGO nanosheets working as an effective cocatalyst. Considering the green and effective method for the reduction of GO, the present investigation can provide new insights into the design and preparation of graphene-based functional composite materials for various potential applications.

## ■ ASSOCIATED CONTENT

### Supporting Information

RD patterns. This material is available free of charge via the Internet at http://pubs.acs.org

## ■ AUTHOR INFORMATION

### Corresponding Author

*E-mail: yuhuogen@yahoo.cn (H.Y.); mlei@bupt.edu.cn (M.L.).

### Notes

The authors declare no competing financial interest.

## ■ ACKNOWLEDGMENTS

This work was partially supported by the National Natural Science Foundation of China (61274129, 21277017, 51208396, 51102019, and 51272031). This work was also financially supported by the 973 Program (2013CB632402, 2010CB923200), 863 Program (2012AA062701) and the natural science foundation of Hubei Province (2012FFB05002).

## ■ REFERENCES

(1) Singh, V.; Joung, D.; Zhai, L.; Das, S.; Khondaker, S. I.; Seal, S. *Prog. Mater. Sci.* **2011**, *56*, 1178.
(2) Novoselov, K. *Rev. Mod. Phys.* **2011**, *83*, 837.
(3) Allen, M. J.; Tung, V. C.; Kaner, R. B. *Chem. Rev.* **2010**, *110*, 132.
(4) Novoselov, K. S.; Geim, A. K.; Morozov, S. V.; Jiang, D.; Zhang, Y.; Dubonos, S. V.; Grigorieva, I. V.; Firsov, A. A. *Science* **2004**, *306*, 666.
(5) Stankovich, S.; Piner, R. D.; Chen, X. Q.; Wu, N. Q.; Nguyen, S. T.; Ruoff, R. S. *J. Mater. Chem.* **2006**, *16*, 155.
(6) Stankovich, S.; Piner, R. D.; Nguyen, S. T.; Ruoff, R. S. *Carbon* **2006**, *44*, 3342.
(7) Park, S.; An, J.; Potts, J. R.; Velamakanni, A.; Murali, S.; Ruoff, R. S. *Carbon* **2011**, *49*, 3019.
(8) Shin, H.; Kim, K. K.; Benayad, A.; Yoon, S.-M.; Park, H. K.; Jung, I.; Jin, M. H.; Jeong, H.; Kim, J. M.; Choi, J.; Lee, Y. H. *Adv. Funct. Mater.* **2009**, *19*, 1987.
(9) Su, C.; Xu, Y.; Zhang, W.; Zhao, J.; Liu, A.; Tang, X.; Tsai, C.; Huang, Y.; Li, L. *ACS Nano* **2010**, *4*, 5285.
(10) Perera, S. D.; Mariano, R. G.; Vu, K.; Nour, N.; Seitz, O.; Chabal, Y.; Balkus, K. J. *ACS Catal.* **2012**, *2*, 949.
(11) Wang, P.; Wang, J.; Wang, X. F.; Yu, H. G.; Yu, J. G.; Lei, M.; Wang, Y. G. *Appl. Catal. B: Environ.* **2013**, *132−133*, 452.
(12) Lou, G. Q.; Jiang, X. J.; Li, M. J.; Shen, Q.; Zhang, L. M.; Yu, H. G. *ACS Appl. Mater. Interfaces* **2013**, *5*, 2161.
(13) Zhang, J.; Yu, J.; Jaroniec, M.; Gong, J. R. *Nano Lett.* **2012**, *12*, 4584.
(14) Dubin, S.; Gilje, S.; Wang, K.; Tung, V. C.; Cha, K.; Hall, A. S.; Farrar, J.; Varshneya, R.; Yang, Y.; Kaner, R. B. *ACS Nano* **2010**, *4*, 3845.
(15) Lin, Z.; Yao, Y.; Li, Z.; Liu, Y.; Wong, C. P. *J. Phys. Chem. C* **2010**, *114*, 14819.
(16) Lv, T.; Pan, L.; Liu, X.; Lu, T.; Zhu, G.; Sun, Z.; Sun, C. Q. *Catal. Sci. Technol.* **2012**, *2*, 754.

(17) Anandan, S.; Narasinga Rao, T.; Sathish, M.; Rangappa, D.; Honma, I.; Miyauchi, M. *ACS Appl. Mater. Interface* **2012**, *5*, 207.
(18) Williams, G.; Seger, B.; Kamat, P. V. *ACS Nano* **2008**, *2*, 1487.
(19) Wu, T. S.; Liu, S.; Luo, Y. L.; Lu, W. B.; Wang, L.; Sun, X. P. *Nanoscale* **2011**, *3*, 2142.
(20) Chatterjee, D.; Mahata, A. *Appl. Catal. B* **2001**, *33*, 119.
(21) Grätzel, M. *Nature* **2001**, *414*, 338.
(22) Chen, C.; Long, M.; Xia, M.; Zhang, C.; Cai, W. *Nanoscale Res. Lett.* **2012**, *7*, 101.
(23) Chen, C.; Cai, W.; Long, M.; Zhou, B.; Wu, Y.; Wu, D.; Feng, Y. *ACS Nano* **2010**, *4*, 6425−6432.
(24) Xu, Y.; Bai, H.; Lu, G.; Li, C.; Shi, G. *J. Am. Chem. Soc.* **2008**, *130*, 5856.
(25) Yu, H. G.; Liu, R.; Wang, X. F.; Wang, P.; Yu, J. G. *Appl. Catal. B* **2012**, *111*, 326.
(26) Yu, H. G.; Liu, L.; Wang, X. F.; Wang, P.; Yu, J. G.; Wang, Y. H. *Dalton Trans.* **2012**, *41*, 10405.
(27) Wang, X. F.; Li, S. F.; Yu, H. G.; Yu, J. G.; Liu, S. W. *Chem.—Eur. J.* **2011**, *17*, 7777.
(28) Wang, X. F.; Li, S. F.; Ma, Y. Q.; Yu, H. G.; Yu, J. G. *J. Phys. Chem. C* **2011**, *115*, 14648.
(29) Fan, Z. J.; Kai, W.; Yan, J.; Wei, T.; Zhi, L. J.; Feng, J.; Ren, Y.; Song, L. P.; Wei, F. *ACS Nano* **2011**, *5*, 191.
(30) Zhang, Y.; Tang, Z.-R.; Fu, X.; Xu, Y.-J. *ACS Nano* **2010**, *4*, 7303.
(31) Abdelsayed, V.; Moussa, S.; Hassan, H. M.; Aluri, H. S.; Collinson, M. M.; El-Shall, M. S. *J. Phys. Chem. Lett.* **2010**, *1*, 2804.
(32) Zangmeister, C. D. *Chem. Mater.* **2010**, *22*, 5625.
(33) Wang, D.; Li, Y.; Wang, Q.; Wang, T. *J. Solid-State Electronchem.* **2012**, *16*, 2095.
(34) Shen, J.; Li, T.; Long, Y.; Shi, M.; Li, N.; Ye, M. *Carbon* **2012**, *50*, 2134.
(35) Li, Q.; Guo, B.; Yu, J.; Ran, J.; Zhang, B.; Yan, H.; Gong, J. R. *J. Am. Chem. Soc.* **2011**, *133*, 10878.
(36) Zhang, M.; Qu, B.; Lei, D.; Chen, Y.; Yu, X.; Chen, L.; Li, Q.; Wang, Y.; Wang, T. *J. Mater. Chem.* **2012**, *22*, 3868.
(37) Kuila, T.; Bose, S.; Khanra, P.; Mishra, A. K.; Kim, N. H.; Lee, J. H. *Carbon* **2012**, *50*, 914.
(38) Hou, C.; Zhang, Q.; Li, Y.; Wang, H. *J. Hazard. Mater.* **2012**, *205−206*, 229.
(39) Xiang, Q.; Yu, J.; Jaroniec, M. *J. Am. Chem. Soc.* **2012**, *134*, 6575.
(40) Luo, D.; Zhang, G.; Liu, J.; Sun, X. *J. Phys. Chem. C* **2011**, *115*, 11327.
(41) Akhavan, O.; Abdolahad, M.; Esfandiar, A.; Mohatashamifar, M. *J. Phys. Chem. C* **2010**, *114*, 12955.
(42) Wang, P.; Wang, J.; Wang, X.; Yu, H.; Yu, J.; Lei, M.; Wang, Y. *Appl. Catal. B: Environ.* **2013**, *132−133*, 452.
(43) Sher Shah, M. S. A.; Park, A. R.; Zhang, K.; Park, J. H.; Yoo, P. J. *ACS Appl. Mater. Interfaces* **2012**, *4*, 3893.
(44) Fan, W.; Lai, Q.; Zhang, Q.; Wang, Y. *J. Phys. Chem. C* **2011**, *115*, 10694.
(45) Li, C. J.; Xu, G. R.; Zhang, B. H.; Gong, J. R. *Appl. Catal. B* **2012**, *115-116*, 201.
(46) Liu, R.; Wang, P.; Wang, X. F.; Yu, H. G.; Yu, J. G. *J. Phys. Chem. C* **2012**, *116*, 17721.
(47) Cao, S.-W.; Yin, Z.; Barber, J.; Boey, F. Y. C.; Loo, S. C. J.; Xue, C. *ACS Appl. Mater. Interfaces* **2011**, *4*, 418.
(48) Wu, T. S.; Wang, K. X.; Li, G. D.; Sun, S. Y.; Sun, J.; Chen, J. S. *ACS Appl. Mater. Interfaces* **2010**, *2*, 544.